Solid-state nanopore channels with DNA selectivity

SAMIR M. IQBAL[1], DEMIR AKIN[1,2] AND RASHID BASHIR[1,2]*

[1]Birck Nanotechnology Center, School of Electrical and Computer Engineering, Purdue University, West Lafayette, Indiana 47907, USA
[2]Weldon School of Biomedical Engineering, Purdue University, West Lafayette, Indiana 47907, USA
*e-mail: bashir@purdue.edu

Published online: 1 April 2007; doi:10.1038/nnano.2007.78

Solid-state nanopores have emerged as possible candidates for next-generation DNA sequencing devices. In such a device, the DNA sequence would be determined by measuring how the forces on the DNA molecules, and also the ion currents through the nanopore, change as the molecules pass through the nanopore. Unlike their biological counterparts, solid-state nanopores have the advantage that they can withstand a wide range of analyte solutions and environments. Here we report solid-state nanopore channels that are selective towards single-stranded DNA (ssDNA). Nanopores functionalized with a 'probe' of hair-pin loop DNA can, under an applied electrical field, selectively transport short lengths of 'target' ssDNA that are complementary to the probe. Even a single base mismatch between the probe and the target results in longer translocation pulses and a significantly reduced number of translocation events. Our single-molecule measurements allow us to measure separately the molecular flux and the pulse duration, providing a tool to gain fundamental insight into the channel–molecule interactions. The results can be explained in the conceptual framework of diffusive molecular transport with particle–channel interactions.

Since the original demonstration of ssDNA passage through α-haemolysin nanopores under an electrical field[1], numerous studies have explored the physics of DNA translocation through these protein-based nanopores[2–4]. In search of more robust devices, techniques for fabricating solid-state nanopores have since been developed[5–7], and the translocation of ssDNA and double-stranded DNA through these structures has been examined[8–10]. One challenge that remains is to devise a means of imparting selectivity to the solid-state nanopores. Recent reports of engineering selectivity in nanopores have included biological nanopores that were selective to various entities of interest[11–13]. Most notably, the use of ssDNA attached in the lumen of an α-haemolysin protein nanopore[13] resulted in longer translocation pulses when a complementary target ssDNA molecule was electrophoretically driven through the nanopore, as compared with a target with a single base-pair mismatch. In the synthetic realm, blocking of background ion current in functionalized gold nanotubes has been reported for single-use selective detection of target proteins[14]. In this study, a protein-based molecular recognition agent was attached to the nanotubes and the corresponding protein target was detected by permanent blockage of the nanotube. For the case of DNA, selective and facilitated transport of ssDNA through gold-plated pores of a filter membrane has been demonstrated. In that report, Kohli *et al.* functionalized the metalized pores with hairpin-loop (HPL) DNA[15] and performed elegant experiments demonstrating enhanced and selective flux of complementary ssDNA through the functionalized nanotubes. They measured the flux after the simultaneous passage of molecules through a large number of pores in a filter membrane. Therefore, single molecule translocation signatures could not be measured using that technique. Here, we provide single-molecule electrophoretic transport measurements of ssDNA through selective nanopores and show that our observations can be explained by appropriate interpretation of the recent theoretical predictions of channel–molecule interactions through nanopores[16].

FABRICATION, FUNCTIONALIZATION AND MEASUREMENTS

We fabricated solid-state nanopore channels (NPCs) for single-molecule DNA detection in thin silicon-on-insulator (SOI) membranes (Fig. 1) using a process described elsewhere[6,7,9]. The approximate dimensions of the NPCs used are given in Fig. 1. The DNA translocation data recording system was similar to what has been described earlier[9]. The NPCs were functionalized with HPL-DNA, similar to an earlier approach[15], but with different sequence and attachment chemistry. The amine-modified HPL-DNA was attached using a bilayer strategy with 3-aminopropyltri-methoxysilane and 1,4-phenylene diisothiocyanate[19]. The proper functionalization conditions yield good DNA attachment to oxide surfaces in nanopores[20]. Under optimal conditions in solution, the HPL-DNA has been shown to demonstrate an all-or-none selectivity down to single-base mismatch sensitivity between perfect complementary (PC) and mismatched (MM) targets[21]. The ssDNA was inserted into the negative electrode chamber and the translocation pulses were recorded. The data were analysed to extract important features including pulse width (τ) and blockage current (I_b) for each case of target sequence. The ssDNA showed no pulses through our NPCs before functionalization, but we always observed well-defined pulses after functionalization of the same pores. This proved that HPL-DNA indeed reduced the effective size of the NPC, down to just a few nanometres or less, consistent with the calculated length of the probe molecules (Fig. 1; see also Supplementary Information,

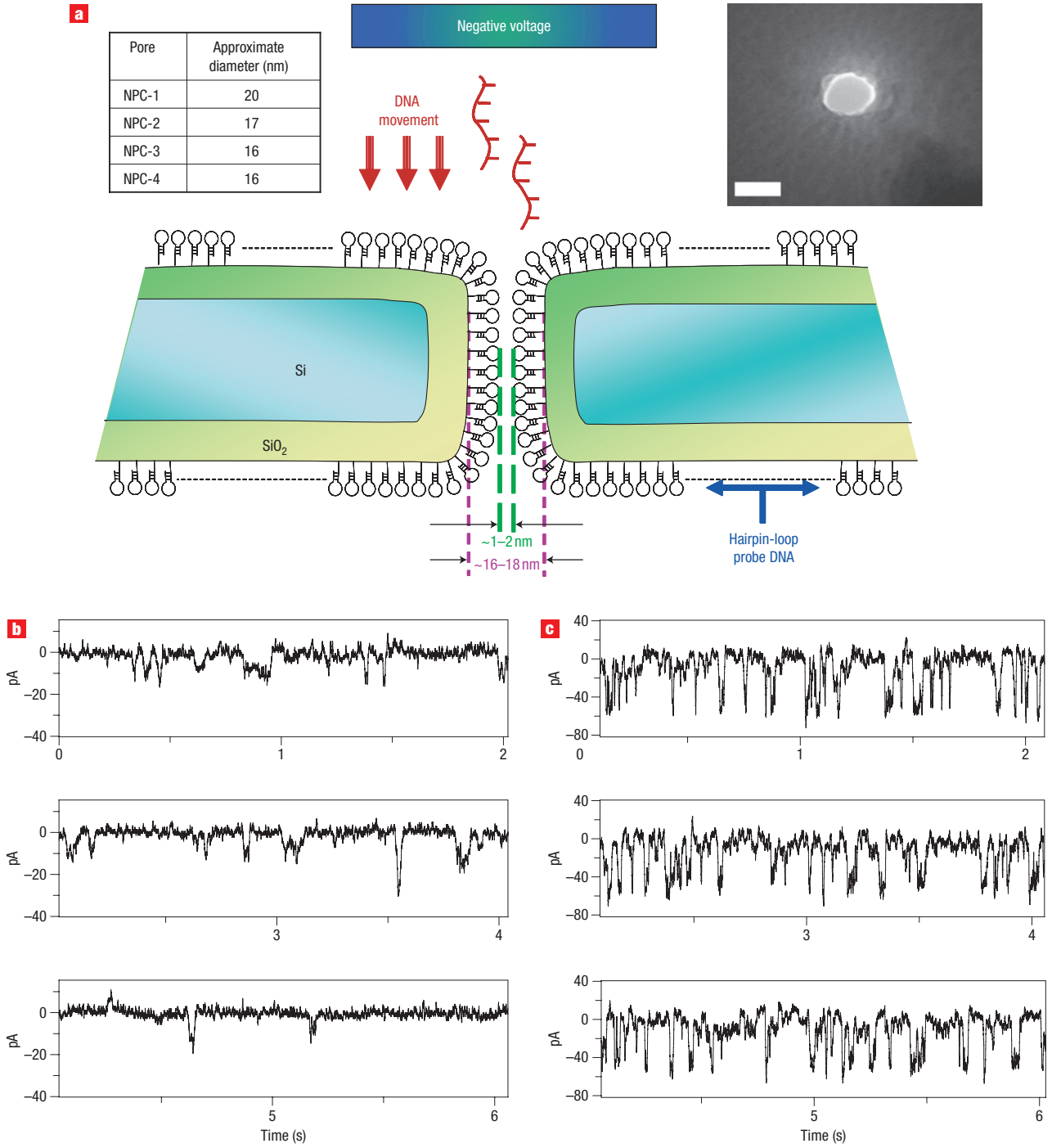

Figure 1 Details of the functionalized NPC sensors. a, Cross-section of the solid-state NPC functionalized with HPL-DNA molecules (not drawn to scale). The inset table shows dimensions of the various NPCs used in this study. The inset TEM image shows the NPC-2 before functionalization (scale bar, 20 nm). **b**,**c**, Current–time representative data for 1MM-DNA (**b**) and PC-DNA (**c**) translocation through NPC-1. A higher number of narrower and deeper pulses are observed for the PC-DNA (**c**) (note change in scale of vertical axes).

Section 2, and Fig. S1). When we used a 40 nm pore, we observed no pulses before or after functionalization as the pore was too big for the current measurement system to detect the blockage. Even after functionalization, the effective pore diameter would be reduced only to ~20 nm. There will therefore be an upper boundary in the size of the NPC, above which it will not function as a selective sensor.

The mismatches in the targets were designed at the stem-forming area and around the stem (Table 1). As shown in the schematic diagram of the functionalized NPC (Fig. 1a), the MM-DNA target tries to traverse the NPC under the applied electrophoretic voltage, while facing electrostatic and mechanical friction and trying to open up the HPL probe to form a duplex. It could be argued that the MM target tries to interact with the

Table 1 List of DNA molecules used in our experiments for functionalization and translocation. The underlined bases indicate the stem-forming part of the probe DNA. The red bases indicate the mismatch.

Type	Sequence
Immobilized hairpin probe	5′-Amine-C6-CCAACGGTTGGTGTGGTTGG-3′
Perfect complement (PC-DNA)	5′-CCAACCACACCAACC-3′
Single-base mismatch (1MM-DNA)	5′-CCAATCACACCAACC-3′
Two-base mismatch (2MM-DNA)	5′-CCAATTACACCAACC-3′
Three-base mismatch (3MM-DNA)	5′-CCATTTACACCAACC-3′

HPL probe unsuccessfully, and, based on earlier works[15] and understanding of molecular transport through channels[16–18], a smaller translocation time for the MM target through the NPC would be predicted, indicating rapid translocation. Very interestingly, we observed the opposite—the single-molecule MM target molecules translocated more slowly (resulting in a larger translocation time) than the PC-DNA molecules. A PC-DNA target should hybridize and bind to the probe inside the channel, resulting in a larger mean residence time and lower diffusion constant than for an MM target (which cannot bind to the probe). Indeed, this was reported for engineered protein nanopores, with one ssDNA probe attached inside the lumen of the pore, providing one molecular recognition site in the small linear dimension[13].

We used the functionalized NPC-1 and introduced the 1MM-DNA target on the side of the membrane with negative potential. The number of pulses per unit time (that is, the flux of DNA molecules traversed) was smaller and the average value of pulse translocation, τ (the mean passage time), was larger, compared with the flux and the mean passage time from subsequent insertion of PC-DNA (after flushing the pore) in the same chamber (Fig. 2, Table 2). The pulses were longer for the 1MM-DNA target, whereas the pulses became clearly shorter for PC-DNA, indicating faster movement of molecules through the NPC. The subsequent reintroduction of 1MM-DNA targets showed that the number of pulses was about the same as before the PC-DNA was passed through the NPC, but the average translocation time was halved (Fig. 2, inset, and Table 2. See also Supplementary Information, Fig. S2). Closer inspection of the data in Fig. 2 further shows that, among the pulses obtained for translocation of 1MM-DNA, there are also narrower pulses (approximate region in dashed circle in the inset) with large blockages, similar to the pulses of PC-DNA. This could be due to that fact that the central pore region in the functionalized NPC-1 still allowed some molecules to pass through without interacting with the HPL probe. This is equivalent to having a weaker attractive potential[16,22], which would reduce the selectivity of the transport by reducing the number of molecules in the NPC at any given time. This hypothesis was verified and the bimodal distribution of the pulses was seen to be removed with the smaller NPC-2, yielding a clearly different distribution of pulses between the 1MM and PC-DNA. As shown in the scatter plot for NPC-2 (Fig. 3), the sequential transport of 1MM-DNA and PC-DNA shows a more selective behaviour, with clearly faster translocation times (lower average τ) and higher blockages (higher average I_b) for the PC-DNA as compared with the 1MM-DNA. Higher blocking currents are also consistent with when a higher percentage of the NPC area is blocked, owing to a smaller pore size, and hence the blockage is more enhanced for the NPC-2 than for the NPC-1. The inset in Fig. 3 shows the 3MM-DNA data recorded before and after the translocation of the PC-DNA. Table 3 shows the statistics for sequential transport of 3MM-, 2MM-, 1MM- PC- and 3MM-DNA through NPC-2. It is interesting to note that after the HPL molecules are opened, even the 3MM-DNA target shows enhanced

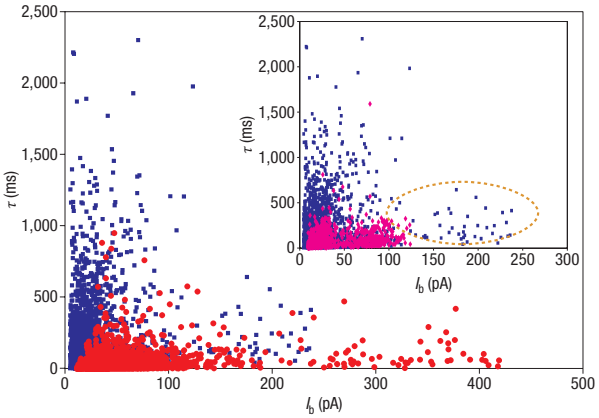

Figure 2 Scatter plot of pulse width versus pulse amplitude for electrophoretic transport of 1MM-DNA and PC-DNA through NPC-1. In the main figure, blue squares represent 1MM-DNA before PC-DNA, and the red circles represent the subsequent passage of PC-DNA. The inset shows a scatter plot of the subsequent passage of 1MM-DNA through the same NPC-1 after the HPL-DNA has opened. Blue squares in the inset are from 1MM-DNA before PC-DNA passed through the NPC-1 (plotted again) and the magenta diamonds are from subsequent passage of 1MM-DNA after the PC-DNA. There were some narrower pulses (elliptical dashed region) with large blockages, similar to the pulses of PC-DNA, from the central pore region allowing molecules to pass through without interaction. Flushing of the NPC with ionic solution (no DNA) was performed before insertion of any molecules.

translocation, with quite a large number of pulses being measured compared with the number before the recognition sites were opened (see Supplementary Information, Fig. S2). This can be putatively attributed to the fact that, in this narrower NPC, the interaction between the target and probe is more pronounced and, once the HPL probe is opened to form a straight duplex with the PC-DNA target, its single-base mismatch selectivity is reduced.

To confirm the validity of our measurements in general, in another experiment with NPC-3, the bias voltage was also changed to 100 mV. The trend was found to be consistent for 200 mV and 100 mV, as τ increased with decreasing bias and the pulse trend (τ, I_b and frequency) stayed the same (see Supplementary Information, Fig. S5). With this NPC, we also investigated the effect of another flushing step between the PC-DNA run and the later translocation of 1MM-DNA. As expected, the 1MM-DNA pulse behaviour after the long PC-DNA exposure became almost identical to that of PC-DNA, consistent with the NPC-1 and NPC-2 trends (see Supplementary Information, Section 6).

Table 2 Summary of the number of translocation pulses, pulse amplitudes and pulse widths for the sequential passage of 1MM-DNA, PC-DNA and 1MM-DNA through NPC-1. The number of measured pulses was scaled to the same measurement time.

NPC-1	1MM-DNA in 120 minutes		PC-DNA in 120 minutes		1MM-DNA after PC-DNA in 120 minutes	
Signature of pulses	τ (ms)	I_b (pA)	τ (ms)	I_b (pA)	τ (ms)	I_b (pA)
Mean	178.8	28.9	10.2	31.2	92.0	29.1
Sigma	260.3	31.7	30.4	27.8	78.2	23.0
Number of pulses	3,353		96,876		2,896	

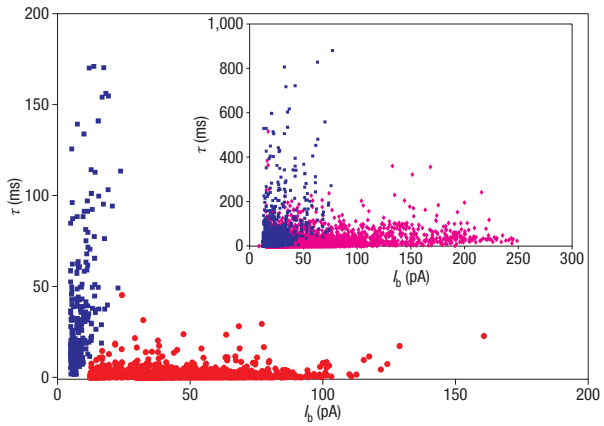

Figure 3 Scatter plot of pulse width versus pulse amplitude for electrophoretic transport of DNA through NPC-2. In the main figure, the blue squares represent 1MM-DNA before PC-DNA and the red circles the subsequent passage of PC-DNA. In the inset, the blue squares represent 3MM-DNA through the same NPC-2 and the magenta diamonds are from the subsequent passage of 3MM-DNA after the PC-DNA. Flushing of NPC with ionic solution (no DNA) was performed before insertion of any molecules.

To elucidate the relaxation (opening) kinetics of the HPL-DNA probe by interactions with a mixture of target DNA and to investigate the temporal viability of such sensors, we measured the pulse behaviour with NPC-4 as a function of time. The target DNA consisted of a 1:1 mixture of 1MM- and PC-DNA by concentration. Figure 4a,b shows scatter plots for the pulses recorded in the first 10 minutes and for minutes 61–70. Quite interestingly, in the beginning, the MM-DNA behaviour was dominating the measured pulses, with a smaller flux (smaller number of pulses per unit time), longer τ and smaller I_b, but, as time progressed, the pulse behaviour shifted towards PC-DNA (with higher flux, smaller τ and longer I_b) (scatter plots for intermediate minute decades can be seen in the Supplementary Information, Fig. S6). This behaviour can be attributed to the HPL being in the closed state at the start of the measurement. Although both molecules interact with the HPL, the flux is limited by the MM-DNA, as the probability of their presence in the repulsive potential is much smaller, and they take longer to pass through the pore. However, PC-DNA do pass through and, as they continue to open the HPL, the flux increases owing to an increased number of both PC- and MM-DNA passing through the NPC. The two regimes of flux are evident in Fig. 4c, and the flux is observed to increase rapidly after about 40 minutes of measurements. The mean passage time also decreases owing to increased facilitation and faster diffusion of the molecules through the NPC (Fig. 4c).

CONCEPTUAL FRAMEWORK

The behaviour of the DNA flux (number of pulses per unit time) and the translocation time can be explained in the conceptual framework of diffusive molecular transport through channels[16–18,22] (for details, see Supplementary Information). In general, the flux of particles translocating through the nanopore channel with no particle–channel interaction can be given by $J_o = (n/\tau)\Delta c$, where n is the number of particles in the channel, or the probability of finding a single particle in the channel for the case of a channel that can be blocked by the particle, τ is the mean passage time or translocation time, and Δc is the difference of concentration across the channel. In the case where there is an attractive channel–molecule interaction (as opposed to no channel–molecule interaction), the flux can increase if the increase in the number of particles dominates over the increase in the mean passage time. Our first assumption is that we can model the interaction of the PC-DNA with the HPL as a case of an attractive potential ($-\phi_{PC}$), and the interaction of the MM-DNA with the HPL as a case of a repulsive potential ($+\phi_{MM}$), as schematically shown in Fig. 5. The HPL-DNA has an all-or-none selectivity towards its target—it interacts and opens up when the target is perfectly complementary and it does not form a duplex with the target if there is even a single base mismatch. There are large electrostatic and mechanical hindrances to the passage of the MM-DNA through the functionalized NPC and hence the interaction can be conceptualized as a repulsive channel–molecule interaction and not as a 'no channel–molecule interaction'. In this case (see Supplementary Information, Section 3), it can be shown that $J_{PC} > J_o > J_{MM}$. Our experimental results clearly show that the number of pulses, that is, the flux, is always lower for the case of MM-DNA and higher for the case of subsequent passage of PC-DNA. Note that we are not comparing the case of attractive potential with that of no potential, but rather with the case of a repulsive potential.

The advantage and uniqueness of our approach is that the direct measurement of the number of pulses and the blockage time allows us to separate the molecular flux and the mean passage time of the molecules to cross the channel. This was not explored in detail in earlier research[13], nor was it possible in earlier measurements[15]. The mean passage time τ, in general, is given by $\tau = (L^2/2D)\langle e^{\phi}\rangle\langle e^{-\phi}\rangle$, which reduces to just $\tau = L^2/2D$ when potential spans over the entire channel length, where L is the channel length, D is the diffusion coefficient, ϕ is the channel potential and $\langle\ \rangle$ represents the statistical average over the channel length. This means that there should be no difference in the mean passage time if the potential spans over the entire length, and the changes in the flux are only due to change in particle number n and not the mean passage time. However, we do observe a clear difference in the τ, and we observe that it is shorter for the PC-DNA/HPL interaction than for the MM-DNA/HPL interaction. This can be explained if we assume that the symmetric potential does not span over the entire length of the channel[16]. In this case, the expression for mean passage time

Table 3 Summary of the number of translocation pulses, pulse amplitudes and pulse widths for the sequential passage of 3MM-DNA, 2MM-DNA, 1MM-DNA, PC-DNA and 3MM-DNA through NPC-2. The number of measured pulses was scaled to the same measurement time.

NPC-2	3MM-DNA in 120 minutes		2MM-DNA in 120 minutes		1MM-DNA in 120 minutes		PC-DNA in 120 minutes		3MM-DNA after PC-DNA in 120 minutes	
Signature of pulses	τ (ms)	I_b (pA)	τ (ms)	I_b (pA)	τ (ms)	I_b (pA)	τ (ms)	I_b (pA)	τ (ms)	I_b (pA)
Mean	32.8	22.4	7.1	23.2	42.9	8.7	0.9	39.6	6.5	28.9
Sigma	69.2	8.6	7.9	10.1	84.4	3.8	1.4	15.9	13.5	17.5
Number of pulses	7,866		15,693		300		238,560		144,076	

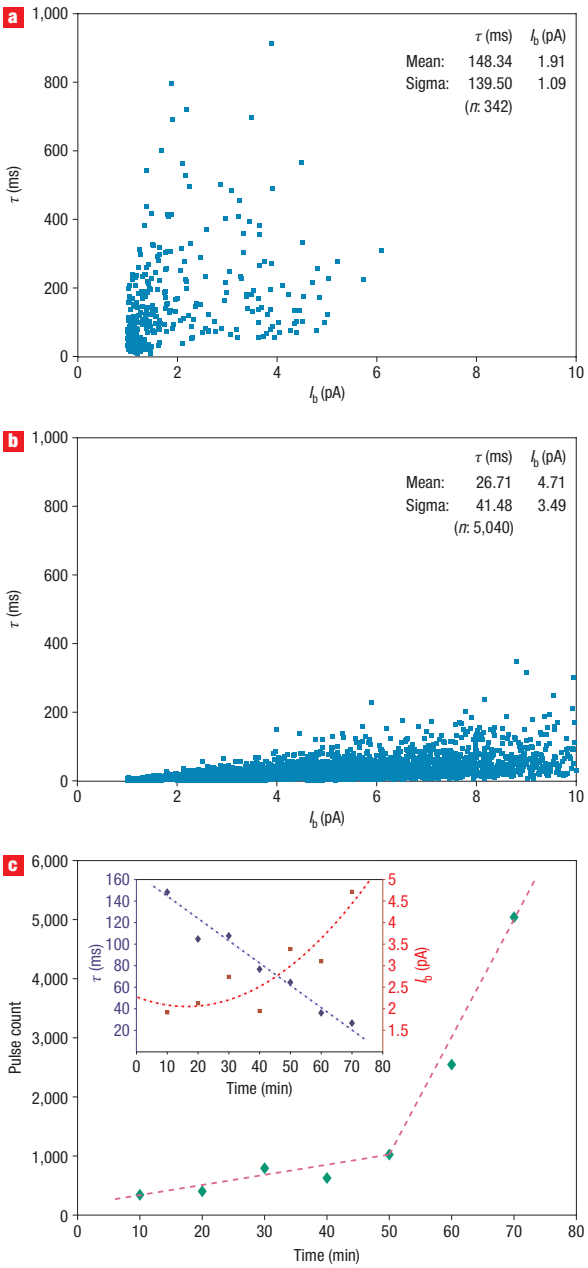

Figure 4 Temporal viability of the NPC-4 with a 1:1 mixture of 1MM-DNA and PC-DNA. a,**b**, Scatter plots of pulse width versus pulse amplitude for electrophoretic transport of the mixture for the first 10 min (**a**) and for minutes 61–70 (**b**). The insets show the statistics for the pulses. **c**, Plot showing the number of pulses recorded summed over intervals of 10 min. The inset shows I_b (red squares) and τ (blue diamonds) versus time, in decades. The lines are plotted to highlight the trends.

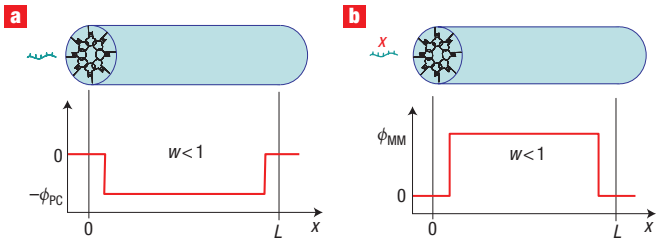

Figure 5 Schematic representation of the potential in the channel. a, An attractive potential spanning over part of the channel, with a PC-DNA interacting with an HPL-DNA. **b**, A repulsive potential spanning over part of the channel, with a 1MM-DNA interacting with HPL-DNA. The concentrations of the baths are c_1 on the $x = 0$ side and c_2 on the $x = L$ side of the channel. The applied electric field, not depicted in these figures, will add a slope to the potential.

is given by $\tau = (L^2/2D)w(1-w)e^{|\phi|}$, where w represents the fraction of the channel encompassed by the potential. The mean passage time for any in-channel potential always increases compared with that of no potential. However, when comparing the case of attractive versus repulsive potentials, the mean passage time could increase or decrease, depending on the magnitude of the potentials, and the ratio of the mean passage times can be given by $\tau_{MM}/\tau_{PC} = e^{|\phi_{MM}|-|\phi_{PC}|}$. This leads to our next assumption, that the magnitude of the repulsive potential is larger than the magnitude of the attractive potential. Again, owing to the all-or-none interaction of the HPL-DNA with its target, this sounds reasonable. We can also attempt to quantify the magnitude of this potential using nearest-neighbour thermodynamic calculations (see Supplementary Information, Section 4). The positive contribution to ΔG_{MM} from the mismatched G and T bases is the root of the repulsive potential that an immobilized HPL-DNA provides to the 1MM-DNA target that tries to interact with it. This can be directly compared with the contributions of the bases at the same place in the PC-HPL duplex, and it can be shown that ΔG_{MM} (at 0.1 M KCl) $\approx 0.93\,\text{kcal mol}^{-1}$, and ΔG_{PC} (at 0.1 M KCl) $\approx -0.6\,\text{kcal mol}^{-1}$. These values of ΔG are consistent with our observed behaviour (Figs 2 and 3, Tables 2 and 3) that the pulse width (that is, the mean passage time) is larger for the translocation of MM-DNA than for the subsequent translocation of the PC-DNA. It should also be noted that the diffusion coefficient used in the above equations of the transit time is not a constant but is indeed dependent on the magnitude of the potential well. As noted in the Supplementary Information, Section 3, the previous analysis assumes an implicit dependence of the diffusion coefficient on the potential. Even if the dependence is explicitly included, the conclusions regarding the change of the mean passage time would still be the same.

Another important aspect to further examine is the behaviour of the NPC as a function of time, as shown in Fig. 4. The PC-DNA opens up the HPL-DNA. These appear to stay open even after the NPCs are flushed with ionic solution, probably because of the steric electrostatic hindrance arising from their confinement in the NPC. The conformational restriction of the surface-tethered strand can be another factor contributing to its inability to reform HPL shape[23]. This surface-tethered behaviour is different from the reformation of HPL in solution, in particular when there are possibilities of G-quartet formation for our HPL-probe[24], as well as cross-hybridizations with other immobilized molecules. The open HPL binding sites are thus available to the MM-DNA when it is reintroduced.

CONCLUSIONS

In general, selective solid-state nanopores such as the ones described here are very attractive, because they have the potential to be stable and robust, and can be realized in an array format. The realization of selective solid-state nanopores can open routes to novel devices for sequencing, detection of single nucleotide polymorphism, expression analysis, and so on, from very few copies of the target DNA molecules, in addition to label-free

detection of proteins or other macromolecules at extremely low concentrations. Clearly, our experimental observations show that it is possible to impart selectivity to solid-state nanopores, and such selectivity can be electrically measured by the translocation signatures at the single-molecule level. In the future, such devices could potentially mimic the exquisite selectivity found in many natural biological channels in cell or nuclear membranes, and help further unravel the physics of selective and facilitated transport of biomolecules in nanoscale channels[25]. Future challenges include developing means for closing the HPL molecules after the interaction with PC-DNA to increase the lifetime of pore selectivity (possibly by appropriate temperature cycling or change in background ionic concentration), being able to make addressable arrays of NPCs where each element is functionalized with a different HPL probe, and direct label-free sequencing and detection of short strands of DNA for many critical applications. The availability of such selective solid-state NPCs also opens up the possibility of detection of specific proteins using the DNA probes and other ligand-receptor systems.

METHODS

NANOPORE CHANNEL FABRICATION

The process flow was adapted from our earlier work[7,9]. The NPCs were fabricated in a Si/SiO_2 membrane on a dual-side polished SOI <100>-oriented p-type wafer. The SOI substrates were used because they provided isolation between the anisotropic etches, which were made independently on both sides of the wafer. The fabrication steps are detailed in the Supplementary Information.

PROBE DNA ATTACHMENT PROCEDURE

The probe DNA molecules were attached to the NPC SiO_2 surfaces using a bilayer scheme. 3-aminopropyltrimethoxysilane was used to form the silane layer, and 1,4-phenylene diisothiocyanate for the homo-bifunctional agent[19]. The 5′-amine-modified probe DNA was prepared at a concentration of 1 pmol μl^{-1} in 1 M Tris–HCl, pH 7.0, containing 1% DPEA. This probe DNA was twice heat-cycled to 10 °C above its melting temperature, with very slow cooling, so all the DNA formed the HPL structure. Details of the attachment process are described in the Supplementary Information.

TARGET DNA SAMPLE PREPARATION

The ssDNA targets had a concentration of 10 pmol μl^{-1} in 10 mM Tris–HCl, pH 8.5, when inserted in the negative-biased Teflon chamber. The target DNA was heat-cycled to 10 °C above its melting temperature, with rapid cooling, to remove any secondary structures in the single strands.

DATA MEASUREMENT AND ANALYSIS

Data recording was started as soon as the target DNA was introduced into the chamber. The ionic solution consisted of 0.1 M KCl, 1 mM Tris–HCl and 0.1 mM EDTA prepared in autoclaved deionized water. Our functionalized NPC chips were sandwiched between O-ring seals and mounted in a measurement system consisting of two ionic-solution-filled Teflon reservoirs separated by the chip[9]. The NPCs were flushed with buffer solution for at least one hour before introducing any type of molecules. All the translocation experiments were carried out at appropriate bias at room temperature. The Teflon blocks and NPCs were placed in a grounded Faraday cage to isolate any electromagnetic noise from the environment. The data were acquired using an SR570 preamplifier from Stanford Research Systems through Ag/AgCl electrodes. The signal was low-pass filtered at a 10 kHz cut-off frequency. A National Instruments data acquisition card (PCI-6024E) was used to generate electrophoretic bias and record data on a personal computer using custom-written LabView software modules. Data were automatically saved in sequential files of either 30 or 60 s duration. An extensive software suite was created to inspect the data and convert them from binary to text format. The text data files were analysed with Clampfit 10 (from the pClamp 10 suite from Molecular Devices Corporation), and plotted using Microsoft Excel.

The time-series ionic current data were analysed using the threshold search feature in the Clampfit software. We defined the threshold as the value above the noise fluctuation of the baseline current. This criterion was consistently applied to the whole analysis. The threshold was set to measure pulse width (τ) and magnitude of blocking current (I_b). The τ was defined as the time difference between the points when the current started dropping, went beyond the threshold value and came back to the base current level. The minimum value of the current during these two points was defined as I_b. The data generated by Clampfit were imported into Microsoft Excel, and scatter plots were obtained. We define a parameter R_P as the ratio of the number of pulses for a MM-DNA target to those of PC-DNA. Figure S2 in the Supplementary Information depicts the change in number of pulses that results due to the activation of the binding sites. The figure also shows the effect of the size of the NPC on increasing sensitivity of our system.

Received 12 January 2007; accepted 1 March 2007; published 1 April 2007.

References

1. Kasianowicz, J. J., Brandin, E., Branton, D. & Deamer, D. W. Characterization of individual polynucleotide molecules using a membrane channel. *Proc. Natl Acad. Sci. USA* **93,** 13770–13773 (1996).
2. Akeson, M., Branton, D., Kasianowicz, J. J., Brandin, E. & Deamer, D. W. Microsecond time-scale discrimination among polycytidylic acid, polyadenylic acid, and polyuridylic acid as homopolymers or as segments within single RNA molecules. *Biophys. J.* **77,** 3227–3233 (1999).
3. Vercoutere, W. A. *et al.* Discrimination among individual Watson–Crick base pairs at the termini of single DNA hairpin molecules. *Nucleic Acids Res.* **31,** 1311–1318 (2003).
4. Mathe, J., Visram, H., Viasnoff, V., Rabin, Y. & Meller, A. Nanopore unzipping of individual DNA hairpin molecules. *Biophys. J.* **87,** 3205–3212 (2004).
5. Li, J. *et al.* Ion-beam sculpting at nanometre length scales. *Nature* **412,** 166–169 (2001).
6. Storm, A. J., Chen, J. H., Ling, X. S., Zandbergen, H. W. & Dekker, C. Fabrication of solid-state nanopores with single-nanometre precision. *Nature Mater.* **2,** 537–540 (2003).
7. Chang, H. *et al.* Towards integrated micro-machined silicon-based nanopores for characterization of DNA. Hilton Head MEMS conference, Hilton Head, South Carolina (2004).
8. Li, J., Gershow, M., Stein, D., Brandin, E. & Golovchenko, J. A. DNA molecules and configurations in a solid-state nanopore microscope. *Nature Mater.* **2,** 611–615 (2003).
9. Chang, H. *et al.* DNA-mediated fluctuations in ionic current through silicon oxide nanopore channels. *Nano Lett.* **4,** 1551–1556 (2004).
10. Smeets, R. M. M. *et al.* Salt dependence of ion transport and DNA translocation through solid-state nanopores. *Nano Lett.* **6,** 89–95 (2006).
11. Gu, L.-Q., Braha, O., Conlan, S., Cheley, S. & Bayley, H. Stochastic sensing of organic analytes by a pore-forming protein containing a molecular adapter. *Nature* **398,** 686–690 (1999).
12. Meller, A., Nivon, L., Brandin, E., Golovchenko, J. & Branton, D. Rapid nanopore discrimination between single polynucleotide molecules. *Proc. Natl Acad. Sci. USA* **97,** 1079–1084 (2000).
13. Howorka, S., Cheley, S. & Bayley, H. Sequence-specific detection of individual DNA strands using engineered nanopores. *Nature Biotechnol.* **19,** 636–639 (2001).
14. Siwy, Z. Troffin, L. Kohli, P. Baker, L. A. Trautmann, C. Martin, C. R. Protein biosensors based on biofunctionalized conical gold nanotubes. *J. Am. Chem. Soc.* **127,** 5000–5001 (2005).
15. Kohli, P. *et al.* DNA-functionalized nanotube membranes with single-base mismatch selectivity. *Science* **305,** 984–986 (2004).
16. Bauer, W. R. & Nadler, W. Molecular transport through channels and pores: Effects of in-channel interactions and blocking. *Proc. Natl Acad. Sci. USA* **103,** 11446–11451 (2006).
17. Noble, R. D., Pellegrino, J. J. & Koval, C.A. Overview of facilitated transport membrane systems. *Chem. Eng. Prog.* **85,** 58–70 (1989).
18. Noble, R. D. Generalized microscopic mechanism of facilitated transport in fixed carrier membranes. *J. Membr. Sci.* **75,** 121–129 (1991).
19. Manning, M., Harvey, S., Galvin, P. & Redmond, G. A versatile multi-platform biochip surface attachment chemistry. *Mater. Sci. Eng. C* **23,** 347–351 (2003).
20. Nilsson, J., Jonathan R. I. L., Ratto, T. V. & Létant, S. E. Localized functionalization of single nanopores. *Adv. Mater.* **18,** 427–431 (2006).
21. Tyagi, S. & Kramer, F. R. Molecular beacons: Probes that fluoresce upon hybridization. *Nature Biotechnol.* **14,** 303–308 (1996).
22. Berezhkovskii, A. M. & Bezrukov, S. M. Optimizing transport of metabolites through large channels: Molecular sieves with and without binding. *Biophys. J.* **88,** L17–L19 (2005).
23. Gao, Y., Wolf L. K. & Georgiadis, R. M. Secondary structure effects on DNA hybridization kinetics: a solution versus surface comparison. *Nucleic Acids Res.* **34,** 3370–3377 (2006).
24. Hamaguchi, N., Ellington A. & Stanton M. Aptamer beacons for the direct detection of proteins. *Anal. Biochem.* **294,** 126–131 (2001).
25. Kasianowicz, J. J., Nguyen, T. L. & Stanford, V. M. Enhancing molecular flux through nanopores by means of attractive interactions. *Proc. Natl Acad. Sci. USA* **103,** 11431–11432 (2006).

Acknowledgements

We acknowledge very useful discussions with M.A. Alam, D.E. Bergstrom and G. Balasundaram (Purdue University), P. Kohli (Southern Illinois University, Carbondale), and also C. Martin (University of Florida) for providing critical input to the conceptual discussion. We are thankful to B.M.K. Venkatesan, H. Chang, E.P. Judokusumo, R. Qaseem and P. Bajaj for help in data analysis. We also thank E.J. Basgall at PSU for electron-beam lithography through the NSF-funded National Nanotechnology Infrastructure Network. Partial wafer fabrication was performed in the Nanotechnology Core Facility at University of Illinois at Chicago. This work was initiated with support from NIH/NIBIB Award No. R21RR15118-01, and subsequently supported by the NASA Institute for Nanoelectronics and Computing at Purdue under Award No. NCC 2–1363.

Supplementary Information accompanies this paper on www.nature.com/naturenanotechnology. Correspondence and requests for materials should be addressed to R.B.

Author contributions

S.M.I. developed the DNA attachment protocols, fabricated the devices, carried out the DNA functionalization and characterization of the devices, and led the measurement and analysis of the data. D.A. identified the DNA probe sequence and helped in developing experiments for the optical characterization of the DNA attachment chemistries. S.M.I. and R.B. designed the experiments and developed the conceptual framework and wrote the paper. R.B. supervised all aspects of the project described above.

Competing financial interests

The authors declare no competing financial interests.